Nat. Hazards Earth Syst. Sci. Discuss., doi:10.5194/nhess-2016-98, 2016
Manuscript under review for journal Nat. Hazards Earth Syst. Sci.
Published: 1 April 2016

Natural Hazards and Earth System Sciences
Discussions

Snow avalanche friction relation based on extended kinetic theory

Matthias Rauter[1,2], Jan-Thomas Fischer[2], Wolfgang Fellin[1], and Andreas Kofler[2]

[1]University of Innsbruck, Institute of Infrastructure, Division of Geotechnical and Tunnel Engineering
[2]Department of Natural Hazards, Austrian Research Centre for Forests (BFW), Innsbruck, Austria

Correspondence to: Matthias Rauter (matthias.rauter@uibk.ac.at)

Abstract. Rheological models for granular materials play an important role in the numerical simulation of dry dense snow avalanches. This article describes the application of a physically based model from the field of kinetic theory to snow avalanche simulations. Those are usually based on depth-averaged two-dimensional models. Therefore a method to adapt the three-dimensional rheological model is presented. In a further step simulation results are compared to velocity and runout observations of avalanches, recorded from different field tests. As reference we utilize a classic phenomenological friction model, which is commonly applied for hazard estimation. The quantitative comparison is based on the combination of normalized residuals of different observation variables in order to take into account the quality of the simulations in various regards. It is demonstrated that the kinetic theory provides a physically based explanation for the structure of phenomenological friction relations and contributes improvements, in particular when different events and various observation variables are investigated.

1 Introduction

Within the last few decades several software tools for the simulation of snow avalanches or, generally speaking, shallow granular flows have been developed, such as SamosAT (Sampl and Zwinger, 2004; Zwinger et al., 2003), TITAN2D (Pitman et al., 2003; Patra et al., 2005), RAMMS (Christen et al., 2010) or r.avaflow (Mergili et al., 2012). In this study the software SamosAT is utilized. The implemented flow model therein is the Savage-Hutter model (Savage and Hutter, 1989, 1991), which is related to the famous shallow water or Saint-Venant equations (de Saint-Venant, 1871). These models idealize avalanches and other free surface flows as depth-averaged flows. The Saint-Venant equations are set up in a Cartesian coordinate system and the normal stresses are assumed to be hydrostatic. On the contrary, the Savage-Hutter equations are set up in a curvilinear coordinate system (compare Bouchut et al., 2004) and the hydrostatic pressure assumption is replaced by an assumption for the lateral active or passive earth pressure, common in soil mechanics. The density is assumed to be constant in both models.

Within this framework rheological models attract a significant portion of attention. A widespread classic phenomenological rheological model used in depth-averaged models is the Voellmy friction model (equation (48)) (Voellmy, 1955). An explanation for the Voellmy friction model, based on a physical model, similar to Bagnold (1954, 1966), is presented in Salm (1993). The Bagnold (1954) model itself can be derived as a specialization of kinetic theory (Mitarai and Nakanishi, 2005; Lee and Huang, 2010).

Buser and Bartelt (2009) introduce the concept of random kinetic energy, similar to granular temperature in kinetic theory. The evolution of the granular temperature is described by a transport equation and influences the rheological behavior, similarly to

Nat. Hazards Earth Syst. Sci. Discuss., doi:10.5194/nhess-2016-98, 2016
Manuscript under review for journal Nat. Hazards Earth Syst. Sci.
Published: 1 April 2016

Natural Hazards and Earth System Sciences Open Access Discussions

the thermodynamic temperature in fluid dynamics. This approach shows some similarities to the kinetic theory model used in this work. However, instead of solving a transport equation, convection and diffusion are neglected and a local equilibrium of the granular temperature is assumed to get an analytical expression for the shear stress. Another approach is presented by Issler and Gauer (2008), who apply the Norem-Irgens-Schiedldrop model (Norem et al., 1987) to deduce a friction relation for snow avalanches.

The rheology of granular materials has been investigated in many scientific works within the framework of three-dimensional continuum mechanics. An important category of microrheological models, dealing with rapid granular flows, is the kinetic theory (Campbell, 1990; Goldhirsch, 2003). Standard kinetic theory struggles to describe the dense flow regime at low shear rates. Recently developed extensions aim to take into account the formation of clusters (Jenkins, 2006, 2007) and enduring force chains (Berzi et al., 2011; Vescovi et al., 2013). The basis of the presented approach is the extended kinetic theory, as formulated by Vescovi et al. (2013). This microrheological model deals with both, the quasi-static regime described by the critical state theory and the rapid, collisional flow, described by the kinetic theory of granular gases.

To implement the constitutive model into the depth-averaged dynamic models, several assumptions about the vertical structure of the flow are made, simplifying the friction relation between avalanche and bottom. It is shown that the simplified expression is similar to classic friction relations. In a further step the obtained relation is compared with classic friction relations, which are often applied in hazard estimation. Therefore back calculations of well-documented avalanches are used to determine minimal residuals in multiple observation variables, such as runout distance, affected area and velocity. It is shown that the relation obtained by kinetic theory allows to reduce the residuals for the presented events.

2 Constitutive relations in the Savage-Hutter model

The governing equations of the Savage-Hutter model, extended for entrainment, as implemented by SamosAT, for an incompressible, granular flow over a one-dimensional terrain can be expressed as

$$\frac{\partial h}{\partial t} + \frac{\partial (h\overline{u})}{\partial x} = \frac{\dot{q}}{\rho}, \tag{1}$$

$$\frac{\partial (h\overline{u})}{\partial t} + \frac{\partial \left(h\overline{u}^2\right)}{\partial x} = h\,g_x - \frac{1}{2\rho}\frac{\partial \left(K_{a/p}\,\sigma_b\,h\right)}{\partial x} - \frac{\tau_b}{\rho}. \tag{2}$$

These expressions can also be written for the two-dimensional case (e.g. Sampl and Zwinger, 2004).

Equation (1) describes the conservation of mass and equation (2) the conservation of momentum parallel to the slope surface. x is the curvilinear coordinate, z the coordinate perpendicular to x and t the time. ρ represents the flows density, assumed to be constant, h the slope perpendicular flow depth, $\overline{u}$ the slope parallel depth integrated velocity of the flow in x-direction $\frac{1}{h}\int_0^h u_x \,\mathrm{d}z$, g_x and g_z are the gravitational accelerations in x- and z-direction, respectively. The entrainment rate $\dot{q}$ represents the mass entrained by the avalanche within a specific amount of time and area (with unit $\mathrm{kg\,m^{-2}\,s^{-1}}$).

The resistance of the material against its deformation is considered with the second and third term on the right-hand side of equation (2). The second term represents the slope parallel pressure gradient $\frac{\partial \sigma_x}{\partial x}$, expressed by the basal normal stress σ_b and the earth pressure coefficient $K_{a/p}$. σ_b is calculated with respect to the centripetal acceleration due to the basal curvature κ as

Nat. Hazards Earth Syst. Sci. Discuss., doi:10.5194/nhess-2016-98, 2016
Manuscript under review for journal Nat. Hazards Earth Syst. Sci.
Published: 1 April 2016

Natural Hazards and Earth System Sciences Discussions

(Sampl and Zwinger, 2004; Fischer et al., 2012)

$$\sigma_b = \rho h \left(g_z + \kappa \overline{u}^2\right). \tag{3}$$

The earth pressure coefficient $K_{a/p}$ is given as

$$K_{a/p} = \begin{cases} K_a = 2\,\dfrac{1-\sqrt{1-\cos^2\phi/\cos^2\delta}}{\cos^2\phi} - 1 & \text{if} \quad \dfrac{\partial \overline{u}}{\partial x} \geq 0 \\ K_p = 2\,\dfrac{1+\sqrt{1-\cos^2\phi/\cos^2\delta}}{\cos^2\phi} - 1 & \text{otherwise} \end{cases}, \tag{4}$$

from a Mohr–Coulomb yield criterion (Savage and Hutter, 1989, 1991). Another approach by Salm (1966, 1993) is based on Rankines earth pressure. Here, ϕ is the internal friction angle and δ the bed friction angle. $K_{a/p} = 1$ coincides with hydrostatic pressure and the Saint-Venant assumption and is a commonly used simplification (Christen et al., 2010). Bartelt et al. (1999) showed, that the sensitivity of the relevant simulation results for snow avalanche modeling to the internal friction angle is rather small. However, a detailed analysis is not in the scope of this work and a fixed internal friction angle, employing equation (4) is utilized.

The third term on the right-hand side of equation (2) describes the basal friction. Usually this term is a combination of a Coulomb type friction ($\sigma_b \tan\delta$) and a velocity dependent drag term ($f(\sigma_b, \overline{u})\,\overline{u}^2$) (Hutter et al., 2005).

3 Constitutive relations in the framework of three-dimensional continuum mechanics

In this section a rheological model formulated within the framework of three-dimensional continuum mechanics is presented. Flows of granular material can display a large span of grain concentrations. Microscopic mechanical processes and consequently the macroscopic behavior of the material changes substantially with the concentration or solid fraction ν and the granular temperature T. They are determined by the flow variables, herein the normal stress along the transversal direction σ and the shear rate $\dot{\gamma}$, given as the derivative of the velocity in its perpendicular direction, $\frac{\partial u}{\partial z}$ (see figure 1). The concentration is defined as

$$\nu = \frac{V_p}{V}, \tag{5}$$

where V_p is the particle volume and V the total volume. The granular temperature is associated with the fluctuation of the particle velocity

$$\frac{3}{2}T = \frac{1}{2}\left(u_p - u\right)^2, \tag{6}$$

where u_p is the particle velocity and u is the mean velocity of the flow. To describe the whole range of flow configurations, multiple mechanical processes, described by different theories, need to be taken into account (Berzi et al., 2011; Vescovi et al., 2013).

On the one hand, the critical state theory (Roscoe et al., 1958; Schofield and Wroth, 1968) describes granular material at

Nat. Hazards Earth Syst. Sci. Discuss., doi:10.5194/nhess-2016-98, 2016
Manuscript under review for journal Nat. Hazards Earth Syst. Sci.
Published: 1 April 2016

Natural Hazards and Earth System Sciences
Open Access
Discussions

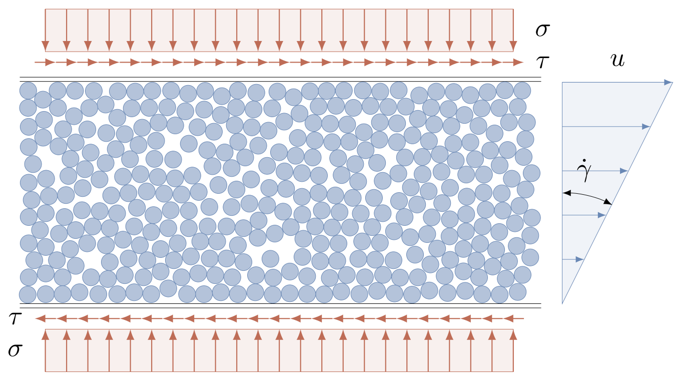

Figure 1. Simple shear flow configuration

vanishingly small shear rates $\dot{\gamma}$. This model is completely time-independent and does not take into account the velocity of any process. The stresses in the material are based completely on enduring force chains between particles. Also the assumption of the incompressibility of granular flows follows from this theory: granular material under motion always reaches asymptotically a certain stress dependent concentration, the critical concentration.
The contribution of quasi-static (subscript q) force chains to the total stresses, as described by the critical state theory, is given as

$$\sigma_q = f_0 \frac{K}{d}, \tag{7}$$

$$\tau_q = \sigma_q \tan\phi'_{ss}, \tag{8}$$

with

$$f_0 = \begin{cases} a\,\dfrac{\nu - \nu_{\mathrm{rlp}}}{\nu_s - \nu} & \text{if and only if } \nu > \nu_{\mathrm{rlp}} \text{ and } \nu_{\mathrm{rlp}} < \nu_s \\ 0 & \text{otherwise} \end{cases}, \tag{9}$$

$$K = \frac{\pi\, d\, E}{8}. \tag{10}$$

Equations (7) and (8) can be considered as critical state line in the ν-σ-τ-space, equation (8) corresponds to the Mohr-Coulomb criterion, both known from soil mechanics. Material parameters are the tangent of the internal friction angle at the critical state $\tan\phi'_{ss}$, the Young's modulus of the particles E, the particle diameter d, the concentration at random loose packing ν_{rlp}, the concentration at closest packing ν_s and the dimensionless parameter a.
On the other hand, the kinetic theory of granular gases describes the granular material under the influence of high shear rates. The stresses in the material are based on short contacts between particles, i.e. elasto-plastic collisions. The following form of this theory was proposed by Garzó and Dufty (1999) and modified by Jenkins and Berzi (2010) and Vescovi et al. (2013). It is limited to homogeneous, steady, simple shear flows of identical, dry, spherical particles.

Nat. Hazards Earth Syst. Sci. Discuss., doi:10.5194/nhess-2016-98, 2016
Manuscript under review for journal Nat. Hazards Earth Syst. Sci.
Published: 1 April 2016

Natural Hazards and Earth System Sciences
Open Access
Discussions

The contribution from collisions (subscript c) to the total stresses is given as

$$\sigma_c = \rho_p\, f_1\, f_4\, T \tag{11}$$

$$\tau_c = \rho_p\, d\, f_2\, f_4\, T^{1/2}\, \dot{\gamma}, \tag{12}$$

and the dissipation rate of the granular temperature by

$$\Gamma_c = \rho_p \frac{f_3}{L}\, f_4\, T^{3/2}, \tag{13}$$

with

$$f_1 = 4\,\nu\, G\, F, \tag{14}$$

$$f_2 = \frac{8\,J}{5\,\pi^{1/2}}\,\nu\, G, \tag{15}$$

$$f_3 = \frac{12}{\pi^{1/2}}\left(1-\epsilon^2\right)\nu\, G, \tag{16}$$

$$G = \nu\, g_0, \tag{17}$$

$$g_0 = \begin{cases} \dfrac{2-\nu}{2(1-\nu)^3} & \nu \leq 0.49 \\ \dfrac{5.69(\nu_s - 0.49)}{\nu_s - \nu} & \nu > 0.49 \end{cases}, \tag{18}$$

$$F = \frac{1+\epsilon}{2} + \frac{1}{4\,G}, \tag{19}$$

$$J = \frac{1+\epsilon}{2} + \frac{\pi}{32}\frac{[5+2\,(1+\epsilon)\,(3\,\epsilon-1)\,G][5+4\,(1+\epsilon)\,G]}{[24-6\,(1-\epsilon)^2-5\,(1-\epsilon^2)]\,G^2}, \tag{20}$$

$$f_4 = \left[1+2\frac{d}{s}\left(\frac{\rho_p\, T}{E}\right)^{1/2}\right]^{-1}, \tag{21}$$

$$s = \frac{\sqrt{2}}{12}\frac{d}{G}, \tag{22}$$

$$f_5 = \frac{L}{d}\frac{f_2}{f_3}, \tag{23}$$

$$\frac{L}{d} = \max\left[1, \left(\frac{c^2\, G^{2/3}\, f_3}{4\, f_2}\right)^{1/3}\right]. \tag{24}$$

Additional material parameters, introduced by the kinetic theory, are the particle density ρ_p, the coefficient of restitution ϵ and the dimensionless parameter c.

The total stresses can be expressed as sum of the quasi-static and the collisional stresses:

$$\sigma = \sigma_q + \sigma_c = \frac{K}{d}\, f_0 + \rho_p\, f_1\, f_4\, T, \tag{25}$$

$$\tau = \tau_q + \tau_c = \frac{K}{d}\, f_0 \tan\phi'_{ss} + \rho_p\, d\, f_2\, f_4\, T^{1/2}\, \dot{\gamma}. \tag{26}$$

The evolution of the granular temperature is described by the conservation equation,

$$\frac{3}{2}\rho\frac{\partial T}{\partial t} = \tau_c\dot{\gamma} - \nabla\cdot\mathbf{q}_c - \Gamma_c, \tag{27}$$

with production $\tau_c\dot{\gamma}$, flux $\mathbf{q}_c$, and dissipation Γ_c. The assumptions of steady state and simple shear imply that granular temperature is dissipated where it has been produced. This approach, called equilibrium assumption (van Wachem, 2000), is also applied to dense flows apart from steady, simple shear conditions in some works (Syamlal et al., 1993; Boemer et al., 1997; van Wachem et al., 1998, 1999; van Wachem, 2000) and is justified by the dominance of generation and dissipation terms over convection and diffusion terms. So the transport equation can be reduced to an algebraic formulation of the equilibrium state, given as (Vescovi et al., 2013)

$$\Gamma_c = \tau_c\dot{\gamma}. \tag{28}$$

This assumption allows to apply the kinetic theory to the dynamic model without introducing additional differential equations, as for example done by Christen et al. (2010).
By introducing equations (12) and (13) into equation (28), the granular temperature can be expressed as a function of the shear rate $\dot{\gamma}$ and the concentration ν:

$$T = d^2 f_5\dot{\gamma}^2. \tag{29}$$

Introducing equation (29) in equations (25) and (26) leads to an expression for the total stresses, only depending on $\dot{\gamma}$ and ν:

$$\sigma = \frac{K}{d}f_0 + \rho_p d^2 f_1 f_4 f_5\dot{\gamma}^2, \tag{30}$$
$$\tau = \frac{K}{d}f_0\tan\phi'_{ss} + \rho_p d^2 f_2 f_4 f_5^{1/2}\dot{\gamma}^2. \tag{31}$$

According to equations (30) and (31), it is possible to characterize the flow regime with only two state variables. In the case of known values for σ and $\dot{\gamma}$, equation (30) can be used to solve for ν, using Newton-Raphson (e.g. Press et al., 1996) or another root-finding routine. τ can then be calculated with equation (31), T with equation (29), if required. Material parameters for snow are not available. To qualitatively highlight the most important features the constitutive model is analyzed for an idealized $1\,\mathrm{mm}$ quartz sand ($d = 1\,\mathrm{mm}$, $\rho_p = 2600\,\mathrm{kg\,m^{-3}}$, $K = 2.8\cdot10^7\,\mathrm{Pa}$, $\epsilon = 0.6$, $c = 0.5$, $a = 1.8\cdot10^{-6}$, $\tan\phi'_{ss} = 0.5$, $\nu_s = 0.619$, $\nu_{\mathrm{rlp}} = 0.55$, Vescovi et al. (2013), see figures 2-8). Figure 2 shows the dynamic critical state surface in the σ-$\dot{\gamma}$-ν-space. According to the presented theory, flow states are limited to this surface. The color in figure 2 shows the dominant source of stresses, which can be interpreted as flow regime. In yellow areas, enduring contacts, forming elastic networks between particles, are dominant (referred to as quasi-static regime (da Cruz et al., 2005; Berzi et al., 2011; Vescovi et al., 2013) or elastic-quasi-static regime (Campbell, 2002, 2005, 2006)). In blue areas, collisional stresses are dominant (referred to as collisional regime (da Cruz et al., 2005; Vescovi et al., 2013; Berzi et al., 2011), kinetic regime (da Cruz et al., 2005; Forterre and Pouliquen, 2008; Vescovi et al., 2013; Berzi et al., 2011) or inertial-collisional regime (Campbell, 2002, 2005, 2006)). The flow is purely collisional for concentrations below the random loose package: $\nu < \nu_{\mathrm{rlp}}$. The red area represents a transitional

Nat. Hazards Earth Syst. Sci. Discuss., doi:10.5194/nhess-2016-98, 2016
Manuscript under review for journal Nat. Hazards Earth Syst. Sci.
Published: 1 April 2016

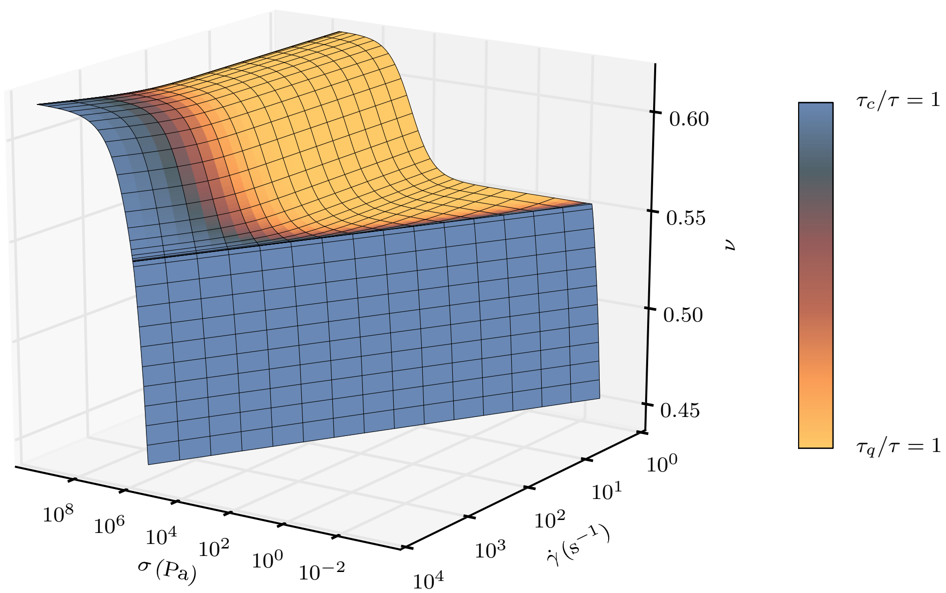

Figure 2. Critical state surface in the σ-$\dot{\gamma}$-ν-space. The color marks the origin of stresses, in yellow areas frictional stresses are dominant, in blue areas collisional stresses.

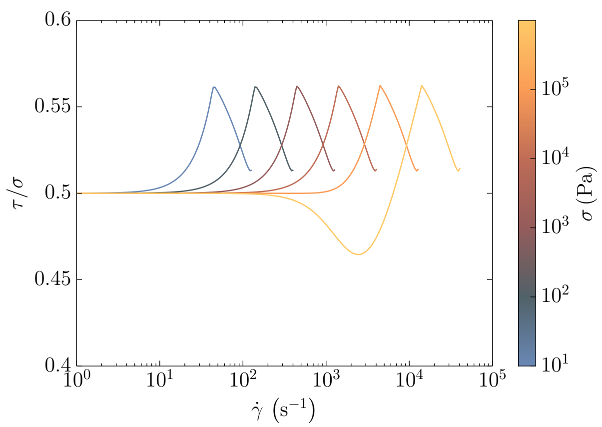

Figure 3. Stress ratio τ/σ in dependence of normal stress σ and shear rate $\dot{\gamma}$

zone between those cases, where both effects co-exist (referred to as dense regime (da Cruz et al., 2005) or elastic-inertial regime (Campbell, 2002, 2005, 2006)).

The granular temperature, which is not shown, is almost solely dependent on the shear rate $\dot{\gamma}$.

The stress ratio τ/σ and the respective concentration ν for a given set of σ and $\dot{\gamma}$ are shown in figure 3 and 4. The constitutive model predicts a stress ratio $\tau/\sigma = \tan\phi'_{ss}$ for $\dot{\gamma} \rightarrow 0$ corresponding to critical state theory and a stress ratio corresponding to kinetic theory for high shear rates. The concentration is almost unaffected by changes in shear rate $\dot{\gamma}$ until it drops below

Nat. Hazards Earth Syst. Sci. Discuss., doi:10.5194/nhess-2016-98, 2016
Manuscript under review for journal Nat. Hazards Earth Syst. Sci.
Published: 1 April 2016

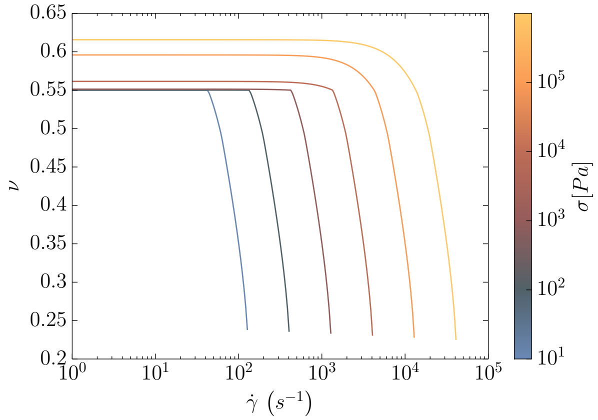

Figure 4. Concentration ν in dependence of normal stress σ and shear rate $\dot{\gamma}$

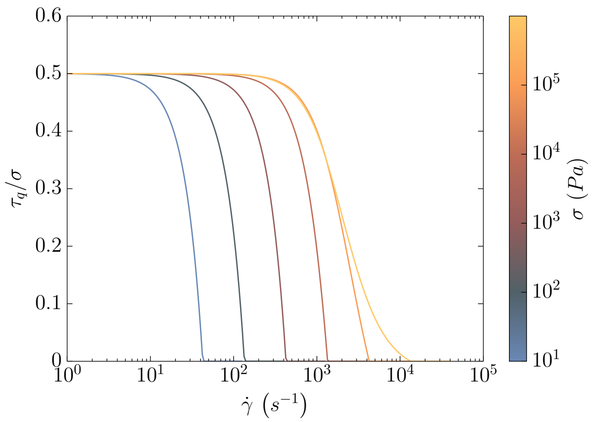

Figure 5. Contribution of enduring force chains: stress ratio τ_q/σ

ν_{rlp}, e.g. at $\dot{\gamma} \approx 5 \cdot 10^2\,\mathrm{s}^{-1}$ for $\sigma = 10^3\,\mathrm{Pa}$. At this point the concentration decreases abruptly and the shear stress lowers with increasing shear rate, after reaching its peak. This behavior can be interpreted as a transition from a dense flow to a powder cloud like flow. This work is focused on dense flow - the post-peak-behavior is therefore not investigated.

A separation of quasi-static and collisional stresses is shown in figures 5 and 6. For small stress levels, increasing collisional stresses τ_c can compensate the decreasing quasi-static stresses τ_q. At high stress levels, this is not the case and the stress ratio $\frac{\tau}{\sigma} = \frac{\tau_q + \tau_c}{\sigma}$ shows a non-monotonic behavior before reaching the peak (figure 3).

This form of constitutive relation is difficult to implement in an operational simulation tool. Therefore approximations of equations (30) and (31) are made. In analogy to other studies (see Ancey (2007) for a review) two approaches, varying the

Nat. Hazards Earth Syst. Sci. Discuss., doi:10.5194/nhess-2016-98, 2016
Manuscript under review for journal Nat. Hazards Earth Syst. Sci.
Published: 1 April 2016

Natural Hazards and Earth System Sciences
Open Access
Discussions

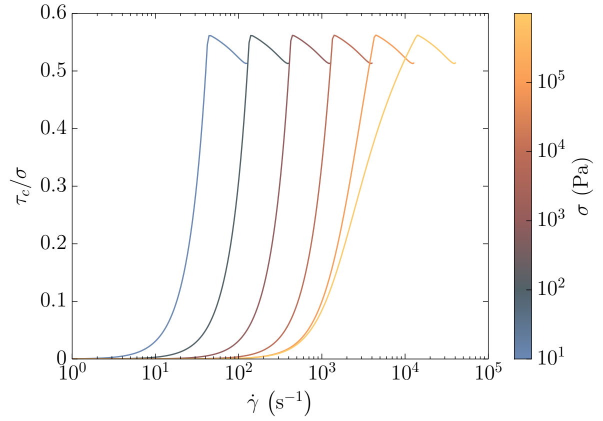

Figure 6. Contribution of collisions: stress ratio τ_c/σ

distribution of collisional and quasi-static friction are evaluated:

$$\tau = \mu(\sigma,\dot{\gamma})\,\sigma + \tilde{\lambda}(\sigma,\dot{\gamma})\,\dot{\gamma}^2, \tag{32}$$

with

$$\mu(\sigma,\dot{\gamma}) = \tan\phi'_{ss}\, f_0, \tag{33}$$

$$\tilde{\lambda}(\sigma,\dot{\gamma}) = \rho_p\, d^2\, f_2\, f_4\, f_5^{1/2}. \tag{34}$$

Within this formulation, $\tilde{\lambda}\,\dot{\gamma}^2$ represents collisional stresses. The decrease of quasi-static stresses is considered with $\mu(\sigma,\dot{\gamma})$. The second approach is given as

$$\tau = \tan\phi'_{ss}\,\sigma + \lambda(\sigma,\dot{\gamma})\,\dot{\gamma}^2, \tag{35}$$

with

$$\lambda(\sigma,\dot{\gamma}) = \rho_p\, d^2\, f_4\, f_5^{1/2}\left(f_2 - f_1\, f_5^{1/2}\tan\phi'_{ss}\right). \tag{36}$$

Here, the term $\lambda\,\dot{\gamma}^2$ also accounts for the decreasing quasi-static stress. Both, $\tilde{\lambda}$ and λ are approximately constant within a certain range of σ and $\dot{\gamma}$. The first approach separates friction by their source (quasi-static - collisional), while the second approach separates friction into a shear-rate independent and shear rate dependent part. The second approach with constant $\mu = \tan\phi'_{ss}$ leads to a better approximation (see figure 7) and a simpler formulation with less parameters. However, the non-monotonic behavior at high stress levels can not be reproduced with this approach. Values for λ are shown in figure 8. Up to a normal stress of 10^4 Pa and until the peak is reached, λ can be approximated as constant. So equation (35) with a constant value for λ is employed in the following:

$$\tau = \mu\,\sigma + \lambda\,\dot{\gamma}^2. \tag{37}$$

Nat. Hazards Earth Syst. Sci. Discuss., doi:10.5194/nhess-2016-98, 2016
Manuscript under review for journal Nat. Hazards Earth Syst. Sci.
Published: 1 April 2016

Natural Hazards and Earth System Sciences
Open Access
Discussions

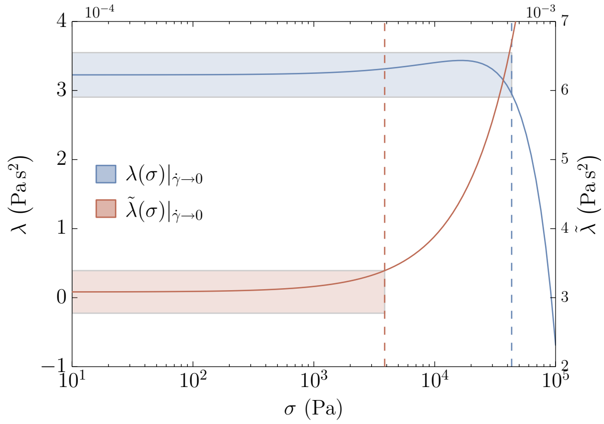

Figure 7. The factors λ (blue) and $\tilde{\lambda}$ (red) for $\dot{\gamma} \to 0$. The colored areas show ranges of σ where the respective value can be approximated with the value at $\sigma \to 0$ within an error of $\pm 10\%$. λ remains in the range of $\lambda|_{\sigma\to 0} \pm 10\%$ up to $4 \cdot 10^4$ Pa, $\tilde{\lambda}$ in the range of $\tilde{\lambda}|_{\sigma\to 0} \pm 10\%$ up to $4 \cdot 10^3$ Pa.

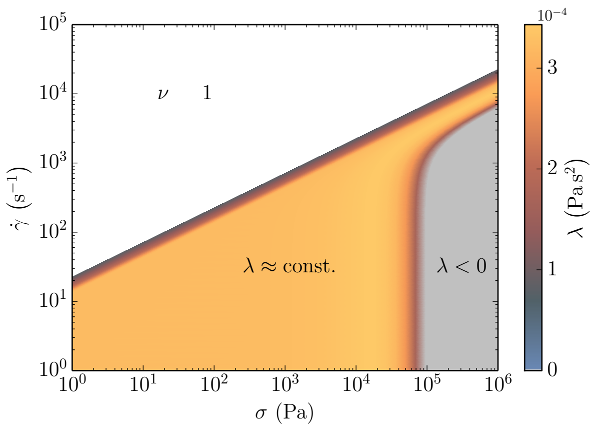

Figure 8. The factor λ as a function of σ and $\dot{\gamma}$. In the white area no solutions could be obtained with the model. In the yellow area the value for the factor λ has its maximum value of approximately $3.5 \cdot 10^{-4}\,\mathrm{Pa\,s^2}$. This value decreases at the borders of the yellow area. In the gray area, values for λ are negative, indicating a non-monotonic behavior.

4 Velocity profile and kinematic relations

The material model obtained by the granular kinetic theory results in a relation depending on the shear rate, which does not explicitly appear in depth-averaged models. However, the equilibrium of stresses at the bottom of the avalanche requires that

$$\tau_b = \tau\left(\sigma_b, \dot{\gamma}_b\right), \tag{38}$$

Nat. Hazards Earth Syst. Sci. Discuss., doi:10.5194/nhess-2016-98, 2016
Manuscript under review for journal Nat. Hazards Earth Syst. Sci.
Published: 1 April 2016

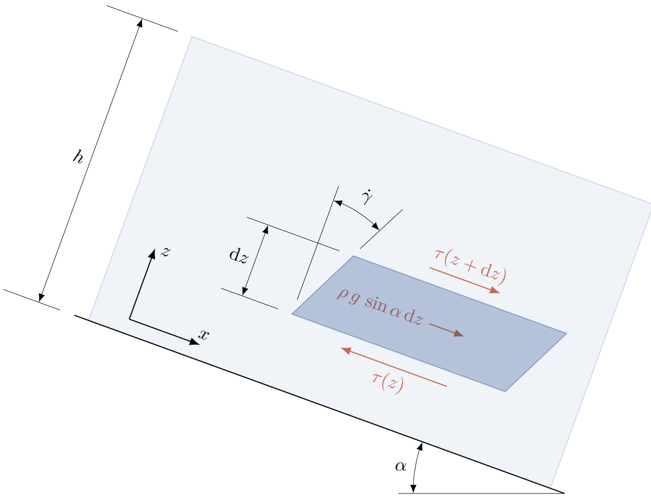

Figure 9. Orientation of the coordinate system and stresses in the slope parallel direction on an infinitesimal small control volume. Slope parallel normal stresses ($K_{a/p}\,\sigma$) cancel each other and are not shown.

where σ_b is the normal stress at the bottom and $\dot{\gamma}_b$ is the shear rate at the bottom. According to the Savage-Hutter model and related friction models, the friction can depend on velocity. To obtain an expression of the form $\tau_b\left(\overline{u},h\right)$ we need to express σ_b (see equation (3)) and $\dot{\gamma}_b$ with known flow variables. Therefore a reconstruction of the velocity profile is required.

Supposing that the avalanche has reached its steady state on a slope with constant inclination α and that $\frac{\partial h}{\partial x}$ is very small, as for the middle part of an avalanche (referred to as equilibrium shape of the velocity profile (Issler and Gauer, 2008) or simple shear infinite landslide model (Dutto, 2014)), all volume forces and stresses can be expressed with the differential equations

$$\frac{\partial \tau}{\partial z} = -\rho\, g \sin\alpha, \tag{39}$$

$$\frac{\partial \sigma}{\partial z} = -\rho\, g \cos\alpha. \tag{40}$$

The left hand side in equations (39) and (40) describes the change of stresses in z-direction, which is caused by the gravitational volume force (right hand side). Introducing the constitutive relation (equation (37)) in equation (39) leads to

$$\frac{\partial}{\partial z}\left(\mu\,\sigma\right) + \frac{\partial}{\partial z}\left(\lambda\,\dot{\gamma}^2\right) = -\rho\, g \sin\alpha, \tag{41}$$

and with equation (40) for $\frac{\partial \sigma}{\partial z}$ to

$$\frac{\partial}{\partial z}\left(\lambda\,\dot{\gamma}^2\right) = \rho\, g\left(\mu\,\cos\alpha - \sin\alpha\right). \tag{42}$$

Integration with respect to the boundary condition $\dot{\gamma}\big|_{z=h} = 0$ (following from $\tau\big|_{z=h} = 0$) leads to

$$\dot{\gamma} = \sqrt{\frac{\rho\, g\left(\sin\alpha - \mu\,\cos\alpha\right)}{\lambda}}\,\sqrt{h-z}. \tag{43}$$

Nat. Hazards Earth Syst. Sci. Discuss., doi:10.5194/nhess-2016-98, 2016
Manuscript under review for journal Nat. Hazards Earth Syst. Sci.
Published: 1 April 2016

Natural Hazards and Earth System Sciences
Open Access
Discussions

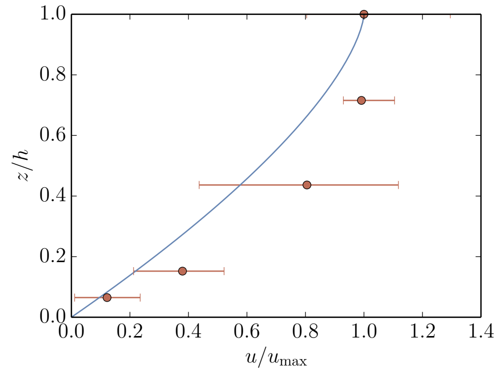

Figure 10. Velocity profile for an infinite avalanche in steady state on a uniformly steep slope for the given rheology model (blue line). For comparison, velocity measurements of a dry snow avalanche from a field test in Vallée de la Sionne is shown (red with error bars) (data from Kern et al., 2009; Sovilla et al., 2015). The measurement shows a more bulbous velocity profile which indicates a plug flow regime. The error bars show the high fluctuation of velocity of grains which agrees to the assumptions of the kinetic theory.

Introducing $\dot{\gamma} = \frac{\partial u}{\partial z}$ and integrating again with respect to the boundary condition $u|_{z=0} = 0$ (no slip condition) leads to an algebraic expression of the velocity profile

$$u = \frac{2}{3}\sqrt{\frac{\rho g\,(\sin\alpha - \mu\cos\alpha)}{\lambda}}\left(h^{3/2} - (h-z)^{3/2}\right). \tag{44}$$

The depth averaged velocity can be calculated with

$$\overline{u} = \frac{1}{h}\int_0^h u(z)\,\mathrm{d}z = \frac{2}{5}\sqrt{\frac{\rho g\,(\sin\alpha - \mu\cos\alpha)}{\lambda}}\,h^{3/2}. \tag{45}$$

Molecular dynamic simulations of granular particles on an inclined plane result in a similar velocity profile, yielding an averaged velocity of $\overline{u} \propto h^{1.52\pm0.05}$ (Silbert et al., 2001). Moreover, this correlation was observed in experiments by Pouliquen (1999). Also a comparison with velocity profile measurements in real scale test sites (Kern et al., 2009; Sovilla et al., 2015) shows resemblance in the middle part of the avalanche, see figure 10.

Finally a relation between the depth averaged velocity (equation (45)) and the shear rate at the bottom of the avalanche $\dot{\gamma}_b = \dot{\gamma}|_{z=0}$ (equation (43)) can be derived:

$$\dot{\gamma}_b = \frac{5}{2}\frac{\overline{u}}{h}. \tag{46}$$

Introducing equation 46 into the constitutive relation leads to the basal shear stress

$$\tau_b = \mu\,\sigma_b + \lambda\left(\frac{5}{2}\right)^2\left(\frac{\overline{u}}{h}\right)^2. \tag{47}$$

The factor $5/2$ is directly related to the shape of the velocity profile and will change for other profiles, e.g. the velocity profile at the front of the avalanche. Moreover, a plug flow near the free surface is not reproduced by equation (47), but visible in the

Nat. Hazards Earth Syst. Sci. Discuss., doi:10.5194/nhess-2016-98, 2016
Manuscript under review for journal Nat. Hazards Earth Syst. Sci.
Published: 1 April 2016

Natural Hazards and Earth System Sciences
Open Access
Discussions

measurement shown in figure 10. Dent et al. (1998) shows velocity profiles where most shearing is concentrated at the ground. The appearance of a plug flow in measurements can be explained with cohesion (Norem et al., 1987), segregation effects or a flow in transitional state (Rauter, 2015). Expression (47) shows some similarities to classic friction relations, the most similar relation is predicted by Issler and Gauer (2008), which is based on the Norem-Irgens-Schiedldrop model (Norem et al., 1987). Also the similarity to the Voellmy friction relation, given as

$$\tau_b = \mu\,\sigma_b + \frac{\rho\,g}{\xi}\,\overline{u}^2, \tag{48}$$

is remarkable. Because of the similarity and its extensive application in snow avalanche simulations, the Voellmy friction model is used as a reference to test the obtained friction relation.

For a better comparison to the Voellmy friction parameter ξ the parameter

$$\chi := \left(\frac{2}{5}\right)^2 \frac{\rho\,g}{\lambda} \tag{49}$$

is introduced. This leads to the expression

$$\tau_b = \mu\,\sigma_b + \frac{\rho\,g}{\chi}\,\frac{\overline{u}^2}{h^2}, \tag{50}$$

where χ contains the velocity profile dependent factor $5/2$. A constant χ indicates, that the same shape of the velocity profile in the whole avalanche is assumed.

The difference between the obtained relation and the friction relation of Voellmy is the inverse quadratic dependency on the flow height. This leads to a lower friction for larger flow heights and therefore larger avalanches. This behavior is in line with observations: To adapt the Voellmy friction model to avalanches of various sizes, different material parameters are used, e.g. μ gets varied between 0.155 for big avalanches and 0.3 for small avalanches, while ξ is usually related to the slope roughness (e.g. Salm et al., 1990; Gruber et al., 1999; Fellin, 2013).

5 Model test and parameter evaluation

To test the obtained friction relation, we employ a multivariate optimization method, based on the work of Fischer et al. (2015). This method takes different optimization variables into account, which represent the main avalanche characteristics, e.g. runout or velocity. These can be obtained from simulation and field observations and their residuals can be quantitatively evaluated. Low absolute residual values indicate a good simulation-observation correspondence. The variation of input parameters is limited to friction parameters, which allows a simple and clear comparison. By scanning the entire physically relevant parameter space, parameter sets, yielding minimal residuals between simulation and observation, are identified. The combination of two different avalanche events, which differ significantly in volume and velocity, are investigated, allowing to unify parameter sets for avalanches of different types, which is usually not only a superposition of the single events (compare Issler et al., 2005). The two avalanche events are (compare Fischer et al., 2014):

Nat. Hazards Earth Syst. Sci. Discuss., doi:10.5194/nhess-2016-98, 2016
Manuscript under review for journal Nat. Hazards Earth Syst. Sci.
Published: 1 April 2016

Natural Hazards and Earth System Sciences
Open Access
Discussions

- Avalanche No. 103 from the 10^{th} of February 1999 at the *Vallée de la Sionne* (VdlS) test site with a deposition volume of approximately $500\,000\,m^3$ and a velocity of up to $70\,\mathrm{m\,s^{-1}}$ (see Sovilla, 2004; Sovilla et al., 2006, for details).
- Avalanche from the 17^{th} of April 1997 at the *Ryggfonn* (Rgf) test site with a deposition volume of approximately $40\,000\,m^3$ and a velocity of up to $40\,\mathrm{m\,s^{-1}}$ (see Gauer et al., 2007, for details).

The simulations have been carried out using the SamosAT simulation software, including entrainment and the respective friction model. To calculate the earth pressure coefficient $K_{a/p}$, a value of $15°$ for the internal friction angle ϕ is used in all simulations. Note that in SamosAT, solving equation (4), ϕ is set equal to δ when $\phi < \delta$.
Especially for the VdlS avalanche, entrainment appears important because of the high increase of volume during its descent. A simple approach for the entrainment rate $\dot{q}$ of the form

$$\dot{q} = \frac{\tau_b}{e_b} |\overline{u}|, \tag{51}$$

where e_b represents the specific erosion energy (compare Fischer et al., 2015) is employed. To estimate appropriate erosion energy coefficients we calculated growth indices, determining the quotient of the deposition mass and the initially released mass. This index is mainly influenced by the entrainment model, the available snow mass and the corresponding parameter. The field observations yield growth indices of 2.3 and 6.0 for Rgf and VdlS, respectively. To resemble values in this range, erosion energy coefficients of $10\,000\,\mathrm{J\,kg^{-1}}$ for Rgf and $1\,000\,\mathrm{J\,kg^{-1}}$ for VdlS, were found to be appropriate. The snow cover height h_{msc}, which is used to limit the entrainment and determine the release volume, was calculated with regards to the elevation and slope inclination α:

$$h_{\text{msc}} = h_0 + \Delta h\,(z - z_{\text{ref}})\cos\alpha, \tag{52}$$

where h_0 represents the snow cover height at the elevation z_{ref} and Δh represents its increase with elevation. This approach ensures a smooth initial snow distribution. The snow cover parameters ($z_{\text{ref}} = 2400\,\mathrm{m}$, $h_0 = 1\,\mathrm{m}$, $\Delta h = 10^{-4}$ for VdlS and $z_{\text{ref}} = 1500\,\mathrm{m}$, $h_0 = 2\,\mathrm{m}$, $\Delta h = 6 \cdot 10^{-5}$ for Rgf) are chosen to match field observations of release volume and snow depth estimates.
In order to investigate the range of possible simulation results, the friction parameter μ is varied uniformly between 0.1 and 0.5 for both friction models, the friction parameters ξ and χ are varied between 10^2 and 10^4 (units are $\mathrm{m\,s^{-2}}$ and $\mathrm{m^{-1}\,s^{-2}}$ respectively). A logarithmic distribution for these parameters is chosen in order to account for the large associated uncertainty, i.e. order of magnitude.
To judge the quality of our simulations they are compared with measurements of the following observation variables:
The velocity in the avalanche track obtained by pulsed Doppler radar measurements. The radar measures the radial velocity and in combination with the elevation model, the surface parallel velocity can be calculated. After an appropriate coordinate transformation these values can then be compared with velocities obtained by simulations (Fischer et al., 2014). The radars settings allowed a distance between range gates of $50\,\mathrm{m}$. This leads to a resolution of 14 values along the avalanche path for both events.

Nat. Hazards Earth Syst. Sci. Discuss., doi:10.5194/nhess-2016-98, 2016
Manuscript under review for journal Nat. Hazards Earth Syst. Sci.
Published: 1 April 2016

Natural Hazards and Earth System Sciences Open Access EGU Discussions

The affected area near the deposition area. The deposition area can not be analyzed directly because the dynamic model does not simulate the deposition process explicitly. Therefore areas, where the simulation results exceed a specific dynamic peak pressure, $p_{\mathrm{lim}} = 1\,\mathrm{kPa}$ in our case, are compared. The pressure is calculated from primary flow variables as

$$p = \rho\overline{u}^2, \tag{53}$$

with $\rho = 200\,\mathrm{kg\,m^{-3}}$. Note that the simulation results are independent of the density ρ and the pressure limit p_{lim} may equivalently be expressed in terms of peak velocities. However, defining affected areas and runout in terms of pressures is in accordance with different international hazard mapping guidelines (c.f. Jóhannesson et al., 2009).

The runout distance along the avalanche path. The runout length is measured as projected length in the natural coordinate system, defined by the avalanche track. Just like the affected area, the runout length is defined by the farthest point where the avalanche exceeds the pressure p_{lim} along its cross section (Fischer, 2013).

To quantify the quality of a simulation with the parameter set i, we used the residuals between values obtained by the respective simulation X_i and the measurements $\hat{X}$, calculated as

$$\delta X_i = \left| X_i - \hat{X} \right|, \tag{54}$$

where δX can be the residual of velocity δu or of runout length δr. The residual of the affected area δA is calculated in a similar manner, but integrated over the investigated area A_{oi}

$$\delta A_i = \int\limits_{A_{\mathrm{oi}}} |a_i(x,y) - \hat{a}(x,y)|\,\mathrm{d}A. \tag{55}$$

Here, $a_i(x,y)$ denotes whether the pressure exceeded the threshold p_{lim} at the respective position x, y in the simulation i or not:

$$a_i(x,y) = \begin{cases} 1 & \text{if} \quad p_i(x,y) \geq p_{\mathrm{lim}} \\ 0 & \text{otherwise} \end{cases}. \tag{56}$$

$\hat{a}(x,y)$ represents the documented affected area in the same manner. Therefore, δA_i represents the area, where simulation and documentation disagree. In this way we could take into account not only the runout distance from a single point, but also the form of the avalanche. The area where the affected area was analyzed (A_{oi}, area of interest, in equation (55)) is shown in figure 11. It contains the whole runout area of all simulations and the documented affected area. To combine residuals expressed by more than one value (like the velocity in the avalanche track, represented by a value for each range gate) we used a value related to the residual sum of squares of the form

$$\delta X_i = \sqrt{\frac{\sum\limits_{n=1}^{N} \delta X_{i,n}^2}{N}}. \tag{57}$$

The division by the number of values N and taking the square root ensures that the resulting residual is of the same unit and of comparable size with respect to the single values. This eases the interpretation from an engineering point of view. We used the same concept to combine residuals from more events to obtain a single residual which would be obtained by simulating these events with the same parameters. The events in this Paper are VdlS and Rgf:

$$\delta X_{i,\text{VdlS+Rgf}} = \sqrt{\frac{\delta X_{i,\text{VdlS}}^2 + \delta X_{i,\text{Rgf}}^2}{2}} \quad (58)$$

To combine residuals of different kinds, like runout and velocity, we normalized the respective residuals with the minimum and maximum residuals from all simulations to eliminate the specific scale

$$\delta X_{i,\text{norm}} = \frac{\delta X_i - \delta X_{\min}}{\delta X_{\max} - \delta X_{\min}}, \quad (59)$$

$$\delta X_{i,\text{comb}} = \sqrt{\frac{\delta \overline{u}_{i,\text{norm}}^2 + \delta r_{i,\text{norm}}^2 + \delta A_{i,\text{norm}}^2}{3}} \quad (60)$$

The normalization was always performed after the combination of values of the same kind and after combining two events. This is important because the normalization and combination of residuals is not distributive.

This method does not require reference values like an acceptable error or a measurement error.

A possible drawback of this method is that larger events have a bigger impact on the results than smaller ones because of the larger absolute values of velocity and runout. If this is not suitable for the respective problem, one could also perform the normalization before combining the events and therefore lay weight on different events equally. The combination of events and measures leads to four possibilities to evaluate and compare model performance with respect to different regards and events (compare figures 13, 14 and table 1):

(a) To a single event with respect to a single observation variable (δr, δA and $\delta\overline{u}$, marked by ▲ ▲ ▲)

(b) To a single event with respect to all investigated observation variables ($\delta r \wedge \delta A \wedge \delta\overline{u}$, marked by ▽)

(c) To both events with respect to a single observation variable ($\delta r_{\text{VdlS+Rgf}}$, $\delta A_{\text{VdlS+Rgf}}$ and $\delta\overline{u}_{\text{VdlS+Rgf}}$, marked by ● ● ●)

(d) To both events with respect to all investigated observation variables ($\delta r_{\text{VdlS+Rgf}} \wedge \delta A_{\text{VdlS+Rgf}} \wedge \delta\overline{u}_{\text{VdlS+Rgf}}$, marked by ○)

The first evaluation is the simplest to be fulfilled sufficiently with the simulation results. The last contains the most information and is therefore the most valuable.

6 Results and Discussion

The following section shows the evaluation of 1 600 simulation runs. This number results from two events, two friction models and 20 values for the friction parameters μ and ξ or χ respectively.

In figure 13 the evaluation of residuals from all simulations is summarized, separated by event and friction model. Figure 14 shows the same result combined for both events. Additionally the combined residuals in dependence of the respective friction parameters are highlighted.

Nat. Hazards Earth Syst. Sci. Discuss., doi:10.5194/nhess-2016-98, 2016
Manuscript under review for journal Nat. Hazards Earth Syst. Sci.
Published: 1 April 2016

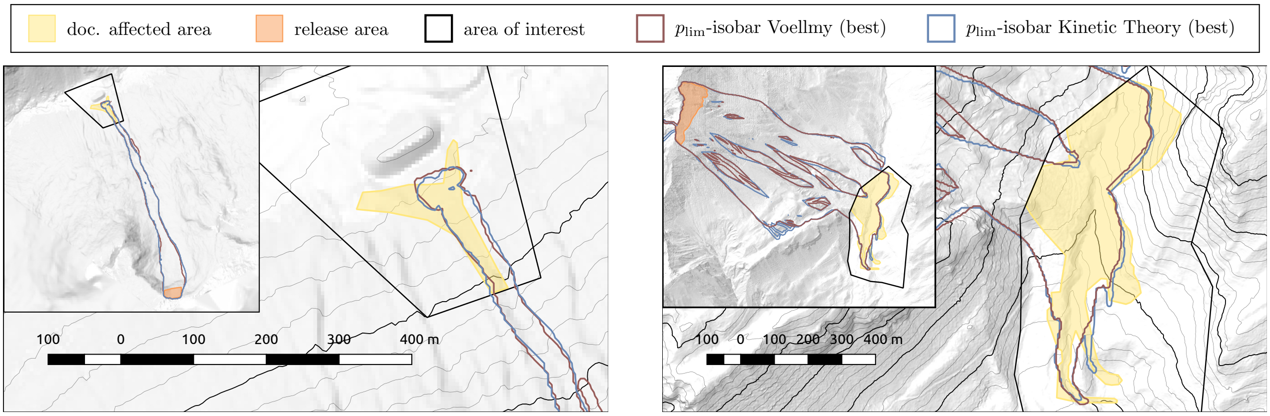

(a) Ryggfonn

(b) Vallée de la Sionne

Figure 11. Outlines of the numerical simulations in comparison with the documented affected area for the avalanche event in Ryggfonn (a) and Vallée de la Sionne (b). The red and blue lines show the p_{lim} isobars for the simulation with the smallest residuals for the Voellmy friction model and the new friction model respectively. The yellow filled areas show the documented affected areas and the orange filled areas show the release areas. The evaluation of the affected area was limited to the area within the black polygons. In the figure showing the event in Rgf one can see that the avalanche (yellow area) stopped and spread apart about $50\,\mathrm{m}$ before the dam. This results from a large snow deposit uphill of the dam. Because the digital elevation model does not take into account the snow height, numerical simulations show the same behavior of the avalanche with an offset of about $50\mathrm{m}$. The smallest residual is achieved by simulations with high friction which leads to a stopping of the avalanche before reaching the dam and an untypical form.

The runout distance represents a point in the avalanche path. Simulations with high friction (high values for μ, low values for ξ and χ) do not reach this point, simulations with low friction exceed this point. Therefore there is a combination of parameters between those limiting cases, where the simulation fits the documented runout length almost perfectly. When optimizing two events together this behavior changes. Two observations need to be satisfied, however, in order to satisfy the two observations each simulation demands its own parameter set. This behavior can be seen in figure 14 as well. The residual for the runout length is $22.9\,\mathrm{m}$ at best when optimizing both events together.

The affected area is also a measure related to runout. However, it provides an additional important information on the lateral extend and spatial distribution of the avalanche. The correlation to runout is clearly visible in figures 13 and 14, as the respective areas of low residuals overlap. Figure 11 shows the documented affected area alongside with the affected area obtained from simulations with the smallest residuals in this respect (δA_{min}). A perfect correspondence between the documented area and the affected area in the simulation does not appear in any of our simulation runs. This can also be seen in figure 13. The smallest residual is about $7\,700\,\mathrm{m}^2$ for Rgf and $65\,000\,\mathrm{m}^2$ for VdlS respectively.

In case of the RGF avalanche, it is observed, that the agreement of documented and simulated affected area is limited. This can be attributed to a large amount of deposited snow in the runout, which is not considered in the digital elevation model, leading to an upstream spreading of the avalanche (see figure 11a). All simulations are affected equally by this effect, which leads to

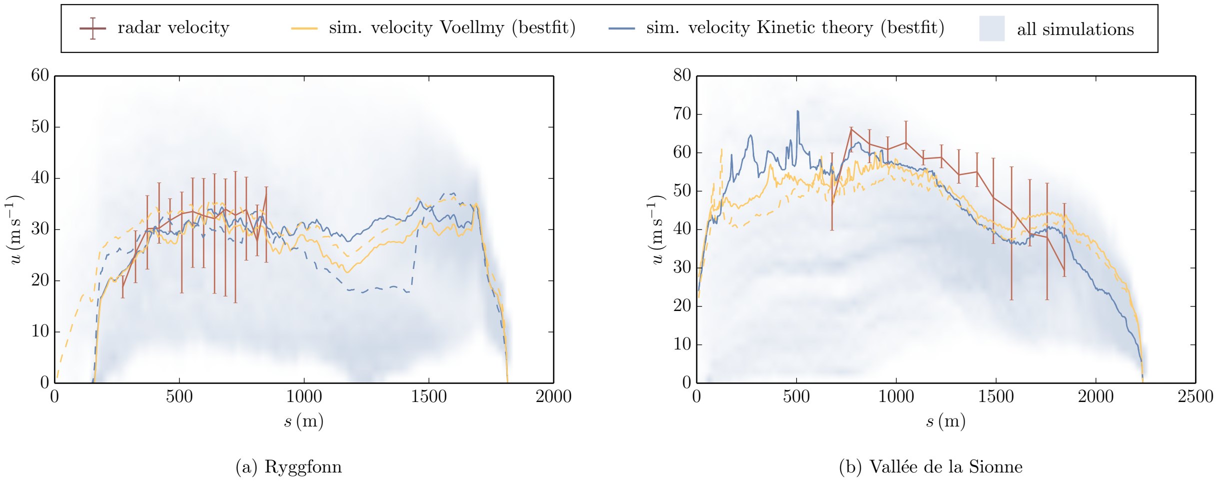

Figure 12. Velocity measurements compared with simulation outcomes for the avalanche event in Ryggfonn (a) and Vallée de la Sionne (b). The flow direction is right to left. The x-axis shows the distance from the radar station, the y-axis shows the velocity. The red line shows the velocity obtained by the pulsed Doppler radar measurements with an estimated observational error. The yellow and blue lines show the velocity along the radar path in the simulation with the smallest residual for the Voellmy friction model and the new friction model respectively. The dashed lines show the best simulation when using the same material parameter for both events. For the kinetic theory friction model the optimized parameter set for VdlS and both events combined coincide. The background shows the distribution of velocities obtained by all simulations.

the big red areas in figures 13a and 13b.

For the event in VdlS, the delineation of the documented affected area is accompanied by uncertainties, due to the large powder cloud of this avalanche. The applied documented affected area represents areas with clearly visible snow depth variations (deposition and erosion) caused by the avalanche (Vallet et al., 2001). Figure 11b shows that simulations with an overall good accordance in the runout fail to reproduce the high climb on the counter slope (the two humps opposite to the two main avalanche tracks). This is the exact area where one expects the powder snow layer to detach from the dense flow layer (the dense flow layer follows the terrain more strictly than the powder snow layer).

Another interesting detail can be observed in figure 11b. In contradiction to the Voellmy model, the kinetic theory model predicts a separation of two branches in the runout zone, which matches the observed behavior. This is an indication for a proper description of important physical processes in the avalanche.

The velocity along the radar path is visualized in figure 12. The residuals are shown in figure 13. For the Rgf event the smallest residual among all simulations is $2.4\,\mathrm{m\,s^{-1}}$ and for the event in the VdlS the smallest residual is $6.2\,\mathrm{m\,s^{-1}}$.

In figure 12a the dashed yellow line, representing the simulation with the smallest residual in velocity for both events combined with the Voellmy model matches the velocity obtained by radar measurements quite well. However, the runout prediction of the respective simulation is inaccurate. This example shows the importance of the evaluation of different observation variables.

The dynamic pressure can be calculated from velocity with equation (53). The residual follows from equation (54) as for other

Nat. Hazards Earth Syst. Sci. Discuss., doi:10.5194/nhess-2016-98, 2016
Manuscript under review for journal Nat. Hazards Earth Syst. Sci.
Published: 1 April 2016

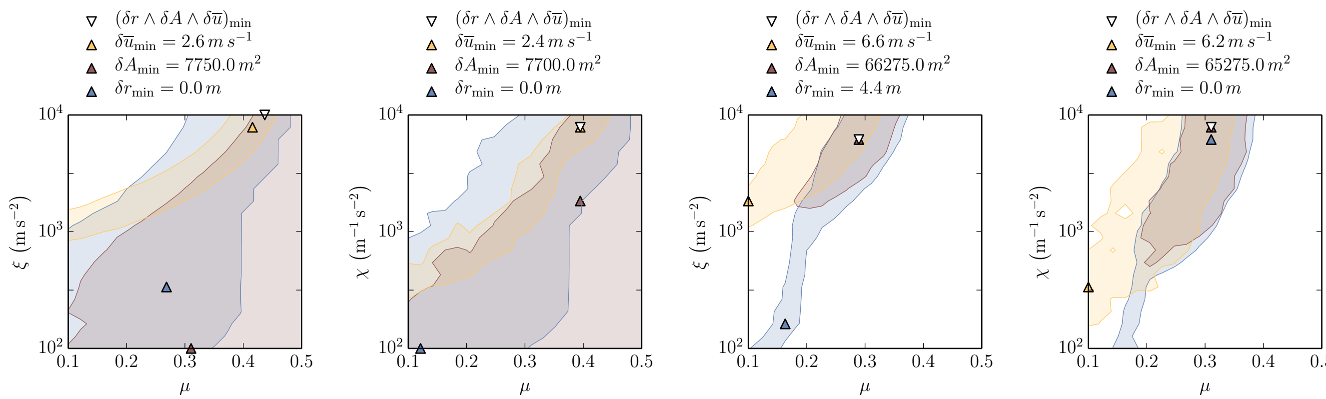

(a) Rgf/Voellmy (b) Rgf/Kinetic theory (c) VdlS/Voellmy (d) VdlS/Kinetic theory

Figure 13. Areas in the parameter space with relatively small residuals (less than 10% on the normalized scale) for the runout length (blue), the affected area (red) and the velocity(yellow) for the different events and friction models. The triangle in the respective color marks the simulation with the smallest residual $\delta X_{\min}$. These residuals correspond to the evaluations of a single variable of a single event (type a). The white triangle marks the smallest combined residual, which corresponds to an evaluation of combined residuals of a single event (type b).

observation variables. A direct calculation of the residual in pressure using the residual in velocity is not possible because of the nonlinear correlation between them. Minimal residuals in velocity yield minimal residuals in pressure of $28\,\mathrm{kPa}$ and $118\,\mathrm{kPa}$ for Rgf and VdlS, respectively. Minimal residuals differ only slightly between the two investigated friction models, when optimizing on single events. However, when using the same set of material parameters for both events, the residual gained with the kinetic theory model is $88\,\mathrm{kPa}$ compared to $116\,\mathrm{kPa}$ from calculation with the Voellmy model (about 25%).

A first impression of possible best fit parameters can be achieved by analyzing the overlapping areas in figure 13. This areas represent parameter combinations which yield relatively small residuals. Figures 14a and 14b show the same kind of areas for a combination of the two events. The bigger influence of the event in VdlS is clearly visible, as figures 14a and 14b are quite similar to 13c and 13d. The white circles in figure 14 mark the positions of the smallest combined residual. In both cases it is located in the overlapping area of relatively small individual residuals.
The combined residual of velocity, runout length and affected area is shown in figures 14c and 14d for both friction models. The minimal combined residual matches the white circle in the above figures. The form of the isobars matches qualitatively the overlapping areas of the above small residuals. The combined normalized residual as calculated here, seems an appropriate method for the determination of optimized parameter sets.

7 Conclusions

From figure 13 one can see, that both rheological models can be fitted almost equally well to single observations from field tests. The smallest residuals differ only slightly for the single cases. When different observation variables are combined, the

Nat. Hazards Earth Syst. Sci. Discuss., doi:10.5194/nhess-2016-98, 2016
Manuscript under review for journal Nat. Hazards Earth Syst. Sci.
Published: 1 April 2016

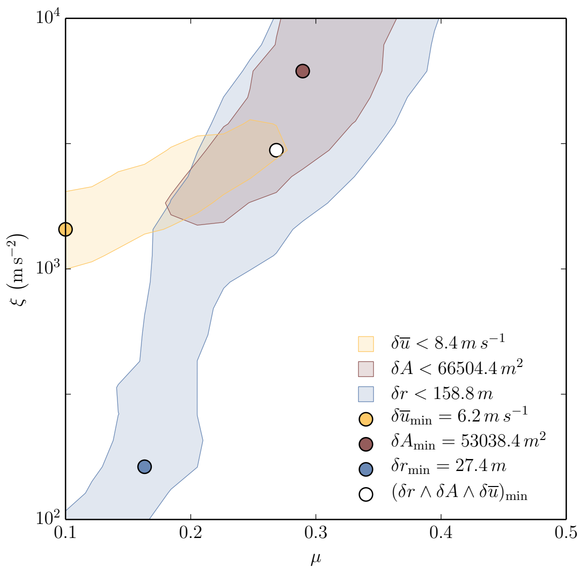

(a) Both events/Voellmy

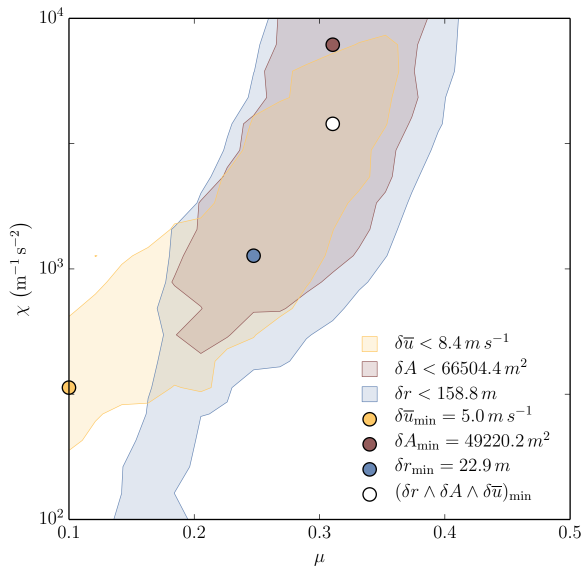

(b) Both events/Kinetic theory

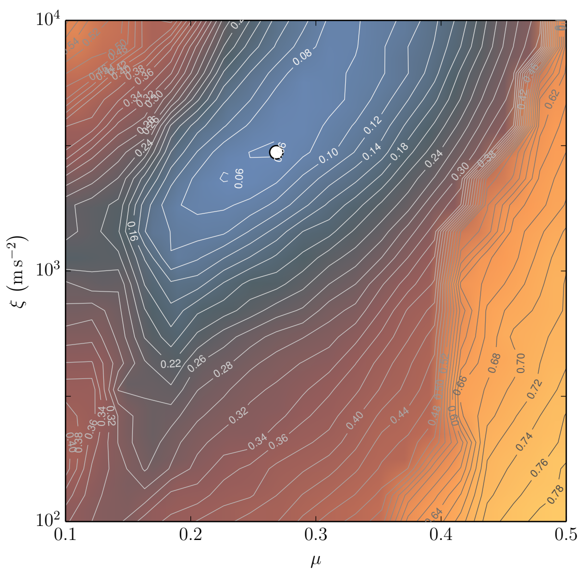

(c) Both events/Voellmy

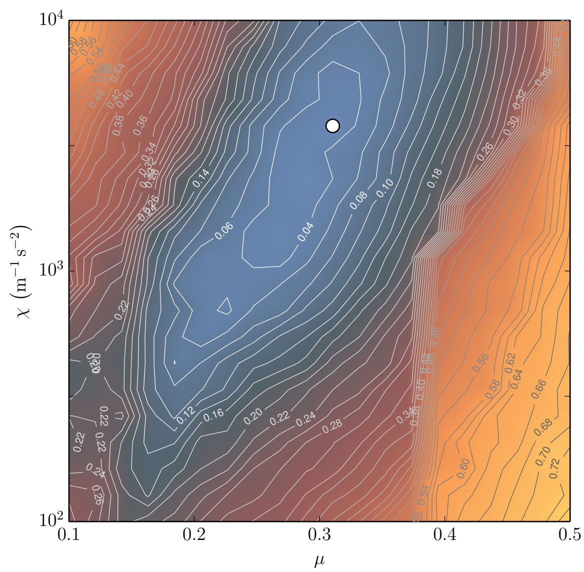

(d) Both event/Kinetic theory

Figure 14. 14a, 14b: Areas in the parameter space with relatively small residuals (less than 10% on the normalized scale) for the runout length (blue), the affected area (red) and the velocity(yellow) for both events combined. The circle in the respective color marks the simulation with the smallest residual $\delta X_{\min}$ (optimization to a single variable for both events, type c). The white circle shows the minimal combined residual of runout, affected area and velocity (optimization type d). 14c, 14d: The combined residual in the parameter space. This surface has a clearly visible local minimum within the physical relevant area. Their position matches with the white circles in the graphs above. The minimal residual is in both cases located within the intersecting areas.

Nat. Hazards Earth Syst. Sci. Discuss., doi:10.5194/nhess-2016-98, 2016
Manuscript under review for journal Nat. Hazards Earth Syst. Sci.
Published: 1 April 2016

Table 1. Obtained residuals for all possible result evaluations. Connected cells are results from the same parameter set. Triangles and circles mark result evaluations which can also be seen in the parameter space in figures 13 and 14 respectively.

method	event	Voellmy			Kinetic Theory			Difference		
		δr	δA	$\delta\overline{u}$	δr	δA	$\delta\overline{u}$	δr	δA	$\delta\overline{u}$
(a)	Rgf	0.0 m	7750 m^2	2.6 m s^{-1}	0.0 m	7700 m^2	2.4 m s^{-1}	0 %	1 %	9 %
(a)	VdlS	4.4 m	66275 m^2	6.6 m s^{-1}	0.0 m	65275 m^2	6.2 m s^{-1}	100 %	2 %	5 %
(b)	Rgf	6.4 m	11675 m^2	2.9 m s^{-1}	12.9 m	10675 m^2	2.4 m s^{-1}	− 100 %	9 %	20 %
(b)	VdlS	13.3 m	66275 m^2	9.3 m s^{-1}	4.4 m	65275 m^2	8.5 m s^{-1}	67 %	2 %	8 %
(c)	Rgf+VdlS	27.4 m	53038 m^2	6.2 m s^{-1}	22.9 m	49220 m^2	5.0 m s^{-1}	16 %	7 %	19 %
(d)	Rgf+VdlS	64.1 m	57779 m^2	8.1 m s^{-1}	24.0 m	49517 m^2	7.0 m s^{-1}	63 %	14 %	13 %

kinetic theory approach allows a better fit to the observed data. This is indicated by the larger overlapping area of the three relatively small residuals in figure 14a compared to the areas in figure 14b. It stands to reason that the modification of the friction with the flow height can help to represent different stages or flow regimes of the avalanche better. This leads to a more realistic dynamic description in different parts of the avalanche, namely the avalanche track and the runout area.

This tendency increases with the number of observations combined. Table 1 shows an overview over possible evaluations and values obtained for both investigated models, where this trend is clearly visible. The difference between the Voellmy model and the kinetic theory model increases with the number of combination in the optimization process. Figure 14 shows residuals of the combination of events. The smallest combined residual for simulations with the Voellmy model is 0.057 (combination of $\delta r = 64\,\mathrm{m}$, $\delta A = 58\,000\,\mathrm{m}^2$, $\delta\overline{u} = 8\,\mathrm{m\,s}^{-1}$ and $\delta p = 159\,\mathrm{kPa}$). The kinetic theory approach reduces this value to 0.020 (combination of $\delta r = 24\,\mathrm{m}$, $\delta A = 50\,000\,\mathrm{m}^2$, $\delta\overline{u} = 7\,\mathrm{m\,s}^{-1}$ and $\delta p = 132\,\mathrm{kPa}$). This corresponds to a reduction of the residual in runout by about 60%, alongside with a reduction of the residual in the pressure along the avalanche track by about 20%.

This improvement can be obtained with very little modification to current models and simulation tools. An additional improvement with a more accurate description of the velocity profile is expected. A more realistic velocity profile should also lead to different friction in head and tail of the avalanche like proposed by Buser and Bartelt (2009).

Overall, velocities predicted by the presented models can match the observations quite well with an optimized set of parameters. However this may also be attributed to the considered entrainment process, since the analysis of similar friction approaches showed less agreement of the velocities, disregarding entrainment (Fischer et al., 2014). This highlights the importance of considering friction and entrainment equally in a process orientated approach and the respective impact on avalanche velocities along the track.

The evaluation of the affected area seems problematic. Part of this problem can be attributed to uncertainties in the documentations. Therefore, it is hard to make assumptions about the quality of the model in this regard.

Another problem of observations in the runout zone is the rising temperature of the avalanche with its descent. The temperature increases because of dissipating kinetic energy and entrainment of warm snow (Vera Valero et al., 2015). This is not considered in the presented rheological model. The possibility of a negative coefficient χ at high pressures, as proposed by the extended kinetic theory, should be further investigated. This effect may help explaining the low friction of catastrophic ice and snow avalanches (Alean, 1985).

In summary this paper highlights how a rheological model from the kinetic theory applies to depth-averaged snow avalanche simulations. To combine both frameworks we employed the commonly accepted assumption of a constant velocity profile along the avalanche and during its decent. The resulting relation shows similarities to classic friction relations. The employed comparison method allowed to evaluate the different basal friction models with respect to different observation variables. Here the residual sum of squares in combination with a normalization, such that values with different physical units and orders of magnitude can be combined, allowed the comparison of the presented friction relation to the wide-spread Voellmy friction relation. Utilizing the new relation shows some improvements, particularly when evaluating different observation variables and multiple events.

Acknowledgements. We would like to express our gratitude to the Norwegian Geotechnical Institute - NGI (P. Gauer) and the WSL Institute for Snow and Avalanche research - SLF (B. Sovilla and P. Bartelt) for collaborative experiments at the Ryggfonn and Vallée de la Sionne test sites and also for access to the respective data and P. Bartelt for fruitful discussions. Furthermore, the authors acknowledge the financial support by the OEAW project "beyond dense flow avalanches".

References

Alean, J.: Ice avalanches: some empirical information about their formation and reach, Journal of Glaciology, 31, 324–333, 1985.

Ancey, C.: Plasticity and geophysical flows: a review, Journal of Non-Newtonian Fluid Mechanics, 142, 4–35, doi:10.1016/j.jnnfm.2006.05.005, 2007.

Bagnold, R.: The shearing and dilatation of dry sand and the 'singing' mechanism, in: Proceedings of the Royal Society of London A: Mathematical, Physical and Engineering Sciences, vol. 295, pp. 219–232, The Royal Society, 1966.

Bagnold, R. A.: Experiments on a gravity-free dispersion of large solid spheres in a Newtonian fluid under shear, in: Proceedings of the Royal Society of London A: Mathematical, Physical and Engineering Sciences, vol. 225, pp. 49–63, The Royal Society, 1954.

Bartelt, P., Salm, L. B., and Gruberl, U.: Calculating dense-snow avalanche runout using a Voellmyfluid model with active/passive longitudinal straining, Journal of Glaciology, 45, 242–254, 1999.

Berzi, D., Di Prisco, C., and Vescovi, D.: Constitutive relations for steady, dense granular flows, Physical Review E, 84, 031 301, doi:10.1103/PhysRevE.84.031301, 2011.

Boemer, A., Qi, H., and Renz, U.: Eulerian simulation of bubble formation at a jet in a two-dimensional fluidized bed, International Journal of Multiphase Flow, 23, 927–944, doi:10.1016/S0301-9322(97)00018-9, 1997.

Bouchut, F., Westdickenberg, M., et al.: Gravity driven shallow water models for arbitrary topography, Communications in Mathematical Sciences, 2, 359–389, 2004.

Buser, O. and Bartelt, P.: Production and decay of random kinetic energy in granular snow avalanches, Journal of Glaciology, 55, 3–12, doi:10.3189/002214309788608859, 2009.

Campbell, C. S.: Rapid granular flows, Annual Review of Fluid Mechanics, 22, 57–90, doi:10.1146/annurev.fl.22.010190.000421, 1990.

Campbell, C. S.: Granular shear flows at the elastic limit, Journal of Fluid Mechanics, 465, 261–291, doi:10.1017/S002211200200109X, 2002.

Campbell, C. S.: Stress-controlled elastic granular shear flows, Journal of Fluid Mechanics, 539, 273–297, doi:10.1017/S0022112005005616, 2005.

Campbell, C. S.: Granular material flows – an overview, Powder Technology, 162, 208–229, doi:10.1016/j.powtec.2005.12.008, 2006.

Christen, M., Kowalski, J., and Bartelt, P.: RAMMS: Numerical simulation of dense snow avalanches in three-dimensional terrain, Cold Regions Science and Technology, 63, 1–14, doi:10.1016/j.coldregions.2010.04.005, 2010.

da Cruz, F., Emam, S., Prochnow, M., Roux, J.-N., and Chevoir, F.: Rheophysics of dense granular materials: Discrete simulation of plane shear flows, Physical Review E, 72, 021 309, doi:10.1103/PhysRevE.72.021309, 2005.

de Saint-Venant, A. J. C. B.: Théorie du mouvement non-permanent des eaux, avec application aux crues des rivières et à l'introduction de marées dans leurs lits., Comptes rendus hebdomadaires des séances de l'Académie des sciences, 73, 147–154, 1871.

Dent, J., Burrell, K., Schmidt, D., Louge, M., Adams, E., and Jazbutis, T.: Density, velocity and friction measurements in a dry-snow avalanche, Annals of Glaciology, 26, 247–252, 1998.

Dutto, P.: Modelling of landslides propagation with SPH: effects of rheology and pore water pressure, Ph.D. thesis, Universidad Politecnica De Madrid, http://oa.upm.es/33166/, 2014.

Fellin, W.: Einführung in Eis-, Schnee-und Lawinenmechanik, Springer-Verlag, 2013.

Fischer, J.-T.: A novel approach to evaluate and compare computational snow avalanche simulation, Natural Hazards and Earth System Science, 13, 1655–1667, doi:10.5194/nhess-13-1655-2013, 2013.

Fischer, J.-T., Kowalski, J., and Pudasaini, S. P.: Topographic curvature effects in applied avalanche modeling, Cold Regions Science and Technology, 74, 21–30, 2012.

Fischer, J.-T., Fromm, R., Gauer, P., and Sovilla, B.: Evaluation of probabilistic snow avalanche simulation ensembles with Doppler radar observations, Cold Regions Science and Technology, 97, 151–158, doi:10.1016/j.coldregions.2013.09.011, 2014.

Fischer, J.-T., Kofler, A., Wolfgang, F., Granig, M., and Kleemayr, K.: Multivariate parameter optimization for computational snow avalanche simulation in 3d terrain, Journal of Glaciology, pp. 875–888, doi:10.3189/2015JoG14J168, 2015.

Forterre, Y. and Pouliquen, O.: Flows of dense granular media, Annual Review of Fluid Mechanics, 40, 1–24, doi:10.1146/annurev.fluid.40.111406.102142, 2008.

Garzó, V. and Dufty, J.: Dense fluid transport for inelastic hard spheres, Physical Review E, 59, 5895–5911, doi:10.1103/PhysRevE.59.5895, 1999.

Gauer, P., Kern, M., Kristensen, K., Lied, K., Rammer, L., and Schreiber, H.: On pulsed Doppler radar measurements of avalanches and their implication to avalanche dynamics, Cold Regions Science and Technology, 50, 55–71, doi:10.1016/j.coldregions.2007.03.009, 2007.

Goldhirsch, I.: Rapid granular flows, Annual Review of Fluid Mechanics, 35, 267–293, doi:10.1146/annurev.fluid.35.101101.161114, 2003.

Gruber, U., Bartelt, P., and Margreth, S.: Anleitung zur Berechnung von Fließlawinen: Neue Berechnungsmethoden in der Lawinengefahrenkartierung, WSL Institut für Schnee-und Lawinenforschung SLF, Davos, 1999.

Hutter, K., Wang, Y., and Pudasaini, S. P.: The Savage–Hutter avalanche model: how far can it be pushed?, Philosophical Transactions of the Royal Society of London A: Mathematical, Physical and Engineering Sciences, 363, 1507–1528, doi:10.1098/rsta.2005.1594, 2005.

Issler, D. and Gauer, P.: Exploring the significance of the fluidized flow regime for avalanche hazard mapping, Annals of Glaciology, 49, 193–198, doi:10.3189/172756408787814997, 2008.

Issler, D., Harbitz, C., Kristensen, K., Lied, K., Moe, A., Barbolini, M., De Blasio, F., Khazaradze, G., McElwaine, J., Mears, A., Naaim, M., and Sailer, R.: A comparison of avalanche models with data from dry-snow avalanches at Ryggfonn, Norway, in: Proc. 11th Intl. Conference and Field Trip on Landslides, Norway, pp. 173–179, Taylor Francis Ltd, 2005.

Jenkins, J. T.: Dense shearing flows of inelastic disks, Physics of Fluids, 18, 103 307, doi:10.1063/1.2364168, 2006.

Jenkins, J. T.: Dense inclined flows of inelastic spheres, Granular matter, 10, 47–52, doi:10.1007/s10035-007-0057-z, 2007.

Jenkins, J. T. and Berzi, D.: Dense inclined flows of inelastic spheres: tests of an extension of kinetic theory, Granular Matter, 12, 151–158, doi:10.1007/s10035-010-0169-8, 2010.

Jóhannesson, T., Gauer, P., Issler, P., and Lied, K.: The design of avalanche protection dams. Recent practical and theoretical developments, No. EUR 23339 in Climate Change and Natural Hazard Research Series 2, 978-92-79-08885-8, 2009.

Kern, M., Bartelt, P., Sovilla, B., and Buser, O.: Measured shear rates in large dry and wet snow avalanches, Journal of Glaciology, 55, 327–338, doi:10.3189/002214309788608714, 2009.

Lee, C.-H. and Huang, C.-J.: Model of sheared granular material and application to surface-driven granular flows under gravity, Physics of Fluids, 22, 043 307, doi:10.1063/1.3400203, 2010.

Mergili, M., Schratz, K., Ostermann, A., and Fellin, W.: Physically-based modelling of granular flows with Open Source GIS, Natural Hazards and Earth System Sciences, 12, 187–200, doi:10.5194/nhess-12-187-2012, 2012.

Mitarai, N. and Nakanishi, H.: Bagnold scaling, density plateau, and kinetic theory analysis of dense granular flow, Physical Review Letters, 94, 128 001, doi:10.1103/PhysRevLett.94.128001, 2005.

Norem, H., Irgens, F., and Schieldrop, B.: A continuum model for calculating snow avalanche velocities, in: Proceedings of the Symposium on Avalanche Formation, Movement and Effects, Davos, Switzerland, pp. 14–19, 1987.

Patra, A. K., Bauer, A., Nichita, C., Pitman, E. B., Sheridan, M., Bursik, M., Rupp, B., Webber, A., Stinton, A., Namikawa, L., et al.: Parallel adaptive numerical simulation of dry avalanches over natural terrain, Journal of Volcanology and Geothermal Research, 139, 1–21, doi:10.1016/j.jvolgeores.2004.06.014, 2005.

Pitman, E. B., Nichita, C. C., Patra, A., Bauer, A., Sheridan, M., and Bursik, M.: Computing granular avalanches and landslides, Physics of Fluids, 15, 3638–3646, doi:10.1063/1.1614253, 2003.

Pouliquen, O.: Scaling laws in granular flows down rough inclined planes, Physics of Fluids, 11, 542–548, doi:10.1063/1.869928, 1999.

Press, W. H., Teukolsky, S. A., Vetterling, W. T., and Flannery, B. P.: Numerical recipes in C, vol. 2, Citeseer, 1996.

Rauter, M.: Entwicklung eines neuen Sohlreibungsmodells für Lawinen, Master's thesis, Universität Innsbruck, Innsbruck, Austria, 2015.

Roscoe, K. H., Schofield, A. N., and Wroth, C. P.: On the yielding of soils, Géotechnique, 8, 22–53, doi:10.1680/geot.1958.8.1.22, 1958.

Salm, B.: Contribution to avalanche dynamics, Symposium at Davos 1965—Scientific Aspects of Snow and Ice Avalanches, 69, 199–214, 1966.

Salm, B.: Flow, flow transition and runout distances of flowing avalanches, Annals of Glaciology, 18, 221–226, 1993.

Salm, B., Gubler, H. U., and Burkard, A.: Berechnung von Fliesslawinen: eine Anleitung für Praktiker mit Beispielen, WSL Institut für Schnee-und Lawinenforschung SLF, Davos, 1990.

Sampl, P. and Zwinger, T.: Avalanche simulation with SAMOS, Annals of glaciology, 38, 393–398, doi:10.3189/172756404781814780, 2004.

Savage, S. B. and Hutter, K.: The motion of a finite mass of granular material down a rough incline, Journal of fluid mechanics, 199, 177–215, doi:10.1017/S0022112089000340, 1989.

Savage, S. B. and Hutter, K.: The dynamics of avalanches of granular materials from initiation to runout. Part I: Analysis, Acta Mechanica, 86, 201–223, doi:10.1007/BF01175958, 1991.

Schofield, A. and Wroth, P.: Critical state soil mechanics, 1968.

Silbert, L. E., Ertaş, D., Grest, G. S., Halsey, T. C., Levine, D., and Plimpton, S. J.: Granular flow down an inclined plane: Bagnold scaling and rheology, Physical Review E, 64, 051 302, doi:10.1103/PhysRevE.64.051302, 2001.

Sovilla, B.: Field experiments and numerical modelling of mass entrainment and deposition processes in snow avalanches, Ph.D. thesis, Swiss Fed. Inst. of Technol., Zurich, http://e-collection.library.ethz.ch/view/eth:27359, 2004.

Sovilla, B., Burlando, P., and Bartelt, P.: Field experiments and numerical modeling of mass entrainment in snow avalanches, Journal of Geophysical Research: Earth Surface, 111, doi:10.1029/2005JF000391, 2006.

Sovilla, B., McElwaine, J. N., and Louge, M. Y.: The structure of powder snow avalanches, Comptes Rendus Physique, 16, 97–104, doi:10.1016/j.crhy.2014.11.005, 2015.

Syamlal, M., Rogers, W., and O'Brien, T. J.: MFIX documentation: Theory guide, National Energy Technology Laboratory, Department of Energy, Technical Note DOE/METC-95/1013 and NTIS/DE95000031, 1993.

Vallet, J., Gruber, U., and Dufour, F.: Photogrammetric avalanche volume measurements at Vallée de la Sionne, Switzerland, Annals of Glaciology, 32, 141–146, doi:10.3189/172756401781819689, 2001.

van Wachem, B. G. M.: Derivation, implementation, and validation of computer simulation models for gas-solid fluidized beds, Ph.D. thesis, TU Delft, Delft University of Technology, Delft, Netherlands, http://repository.tudelft.nl/assets/uuid:919e2efa-5db2-40e6-9082-83b1416709a6/as_wachem_20000918.PDF, 2000.

van Wachem, B. G. M., Schouten, J. C., Krishna, R., and van den Bleek, C. M.: Eulerian simulations of bubbling behaviour in gas-solid fluidised beds, Computers & chemical engineering, 22, 299–306, doi:10.1016/S0098-1354(98)00068-4, 1998.

van Wachem, B. G. M., Schouten, J. C., Krishna, R., and van den Bleek, C. M.: Validation of the Eulerian simulated dynamic behaviour of gas–solid fluidised beds, Chemical Engineering Science, 54, 2141–2149, doi:10.1016/S0009-2509(98)00303-0, 1999.

Vera Valero, C., Wikstroem Jones, K., Bühler, Y., and Bartelt, P.: Release temperature, snow-cover entrainment and the thermal flow regime of snow avalanches, Journal of Glaciology, 61, 173–184, doi:10.3189/2015JoG14J117, 2015.

Vescovi, D., di Prisco, C., and Berzi, D.: From solid to granular gases: the steady state for granular materials, International Journal for Numerical and Analytical Methods in Geomechanics, 37, 2937–2951, doi:10.1002/nag.2169, 2013.

Voellmy, A.: Über die Zerstörungskraft von Lawinen., Schweizerische Bauzeitung, 73, 1955.

Zwinger, T., Kluwick, A., and Sampl, P.: Numerical Simulation of Dry-Snow Avalanche Flow over Natural Terrain, in: Dynamic Response of Granular and Porous Materials under Large and Catastrophic Deformations, edited by Hutter, K. and Kirchner, N., vol. 11 of *Lecture Notes in Applied and Computational Mechanics*, pp. 161–194, Springer Berlin Heidelberg, doi:10.1007/978-3-540-36565-5_5, 2003.